Journal of Materials and Engineering Structures

Research Paper

Using optimization algorithms to detect damages on free-free beam based on dynamic results

Quoc-Bao Nguyen [a,*]

[a] *Department of Bridge and Road Engineering, Hanoi University of Civil Engineering, 55 GiaiPhong Road, Hanoi 100000, Vietnam*

ARTICLE INFO

Article history :

Received 3 March 2023

Revised 24 April 2023

Accepted 24 May 2023

Keywords:

Damage detection

Natural frequency

Optimization

Free-free beam

ABSTRACT

This article describes a Modal Analysis method for detecting damage in free-free beams using natural frequency data. The method involves updating a numerical model of the beam with experimental or reference natural frequencies to determine the damage location and damage index. The accuracy of the method was verified through simulations and experiments on beams with both single and double damage zones. The results demonstrate that the method is effective in detecting the damage location for single damage zone and double damage zones with the same or different damage index. However, when the two damage zones are close together, the method that updates the model through PSO optimization algorithm using the reference frequency data may produce inaccurate results. Furthermore, when using experimental frequency data for damage beams, the results indicate that the method has a damage location error of approximately 3.5% along the entire beam length, which is considered acceptable in practical applications. The natural frequency-based damage detection method described in this article offers a useful tool for the assessment of damage in free-free beams and can be effectively combined with visual inspection techniques.

1 Introduction

The durability and strength of construction structures, such as buildings, bridges, ports, sports fields, and others, can often deteriorate over time due to various factors such as aging, wear and tear, and environmental exposure. This deterioration can lead to the emergence of structural defects, which can compromise the stability and safety of the structure. These defects can arise from various sources, including poor design, subpar materials, construction errors, and environmental factors. At first, these structural defects may not have a noticeable impact on the functionality of the structure. However, as time goes on, these defects can gradually become more severe and pose a significant threat to the safety and stability of the structure. Early detection of these defects is crucial for reducing the risk of damage and ensuring the longevity of the structure. Timely detection of structural defects can also have a significant impact on the cost of repairs and maintenance. If the defects are detected early, they can be repaired at a relatively low cost, allowing the structure to continue to be used as intended. However,

* *Corresponding author. Tel.: +84 988825559.*
E-mail address: baonq@huce.edu.vn

e-ISSN: 2170-127X,

RESEARCH REVIEW of Sciences and Technologies

if the defects are not detected in a timely manner, the cost of repairs can skyrocket, and the structure may need to be temporarily closed for repairs, leading to significant financial losses. For these reasons, it is imperative that efforts are made to regularly assess the health of construction structures and identify any structural defects before they become severe.

For identifying damage in structures, Visual Inspection is the simplest and most straightforward method. A trained inspector will physically examine the structure and look for visible signs of damage such as cracks, deformations, and other physical signs of stress. This method is particularly useful in identifying surface damage and is frequently combined with other methods to confirm or validate results [1-4]. Another commonly used method Ultrasonic Testing, which involves using ultrasonic waves to detect internal defects and cracks. This method works by sending an ultrasonic wave into the material and measuring the time it takes for the wave to travel through the material and return to the surface. This allows determining the presence of any internal defects [5-7]. Impact-Echo Testing is a non-destructive testing method that involves tapping the surface of a building structure and measuring its response. The method works by measuring the echoes of the impact, which can provide information about the location and index of damage within the structure. This method is particularly useful for detecting damage in concrete structures and can be used to identify cracks, voids, and other defects [8-11]. X-ray and Computed Tomography (CT) scans are imaging techniques that can be used to create images of the interior of a building structure. These methods use X-rays or CT scans to create detailed images of the building, which can be used to identify internal damage such as cracks and other defects [12-15]. Thermography involves using infrared cameras to detect temperature changes on the structure surface. This method can be used to identify damage within the structure by looking for areas where the temperature is significantly different from the surrounding areas. This method can be particularly useful for identifying damage that is not visible to the naked eye, such as damage deep within the structure [16-18]. Ground-Penetrating Radar (GPR) is a method that uses radar technology to create images of the subsurface of a building structure. This method can be used to identify hidden damage, such as damage to the foundation or underground structures. GPR works by sending radar waves into the ground and measuring the time it takes for the waves to travel pass the material and return to the surface. The time it takes for the waves to return can be used to create images of the subsurface and identify any damage [19, 20]. Structural Health Monitoring (SHM) involves the use of sensors and monitoring systems to continuously monitor a building structure for changes in behavior that may indicate damage. This method can be used to identify damage early on, before it becomes more severe, and can be particularly useful for monitoring large, complex structures over time. The sensors used in SHM can measure a variety of parameters, including displacement, strain, and acceleration, which can provide information about the overall health of the structure, [21-28]. Structure health is diagnosed by comparing different states of the structure at different times, which become the main assumption in many recent studies [29-38].

Among the methods mentioned, the SHM method based on vibration measurement data is increasingly used due to its advantages in early damage detection, ease of application, and most importantly, it is a non-destructive method. There are several methods for determining structural damage using SHM and dynamic measurement data, each with its own advantages and disadvantages. Modal Analysis is a method that identifies changes in the structure dynamic behavior by analyzing its natural frequencies, mode shapes, and damping ratios. This method compares the changes in the modal parameters of a structure to a reference model in order to detect the presence of damage. Modal analysis is widely used in SHM because it is relatively easy to implement and it provides a good representation of the structure global behavior [39-44]. Nahvi and Jabbari [39] proposed a method to determine the location and depth of crack in a uniform cantilever beam using modal analysis based on natural frequencies and mode shapes. Their findings revealed that the crack location and size have a noticeable effect on the first and second natural frequencies; the natural frequencies decrease significantly as the crack location moves towards the fixed end of beam. In another study [40], Modal Analysis was employed based on the natural frequency and mode shape of the first five modes. An anomaly detection machine learning algorithm was proposed to train a statistical model on the reference healthy state, establish a threshold between healthy and damaged states, and validate the algorithm using independent testing data sets. This algorithm could distinguish healthy and damaged states, even in situations where modal frequencies are indistinguishable between mentioned states. In another study, Cao el al. [43] opted to use an integrated highspeed camera system to identify vibrational features, instead of accelerometer sensors. As a result, they proposed a novel damage localization method that can localize damage without requiring baseline-data of the intact state. Comparing the results obtained from the accelerometers with those obtained from the high-speed cameras confirms the accuracy of using image-based measurements to determine the location and intensity of damage [42]. Time-History Analysis is a method that uses time-domain data, such as acceleration, velocity, and displacement, to identify changes in a structure's behavior over time. This method analyzes changes in the dynamic behavior of a structure to determine the presence and location of damage. Time-history analysis is useful because it provides a detailed description of the structure's response over time, making it possible to detect small changes in its behavior [45, 46]. Frequency-Response Analysis analyzes frequency-domain data,

such as frequency response functions (FRF), to determine the presence of damage in a structure. This method uses the structure's FRFs to identify changes in its natural frequencies and mode shapes. Frequency-response analysis is often used in SHM because it provides a good representation of the structure's global behavior and is relatively easy to implement [47, 48]. Stochastic Subspace Identification (SSI) uses a statistical approach to identify changes in a structure's dynamic behavior. This method uses a mathematical model to analyze changes in the structure's frequency response and to determine the presence of damage. SSI is a powerful method for SHM because it is able to identify damage even in the presence of measurement noise and it provides a good representation of the structure's global behavior [49, 50]. Damage Index Method is a method that uses a numerical index to represent the extent of damage in a structure. This method compares the current behavior of a structure to a reference model to determine the presence and extent of damage. The damage index method is easy to implement and it provides a clear representation of the extent of damage in a structure [51, 52]. Artificial Neural Network (ANN) and Machine Learning (ML) based Methods use artificial intelligence techniques to identify changes in a structure's dynamic behavior. These methods use data from sensors to train a machine learning model, which can then be used to identify changes in the structure's behavior. ANN and ML based methods are useful for SHM because they can handle large amounts of data and identify changes in the structure's behavior that are difficult to detect using other methods [53, 54].

This paper uses the Modal Analysis method to identify the location of damage and assess the severity of damage in a free-free steel beam. The experimental model is a 1 m long with a cross section of 0.07 x 0.01 m. The Matlab-based numerical model was validated through comparison with experimental results. The method was tested on numerical models of beams with one and two failures, at various levels of damage. Subsequently, several tests were conducted on damage beam to evaluate the effectiveness of the Model analysis method under practical conditions.

2 Basis idea

The basic idea of determining the damage characteristics of a free-free beam is to use a model updating method based on the optimization algorithms [55-60]. The procedure consists of the following steps:

- **Step 1 - Intact free-free beam experiment:** Construct an experimental model and determine the experimental natural frequencies of the intact free-free beam.

- **Step 2 - Validation of numerical model:** Establish a numerical model of the intact free-free beam and compare its vibration characteristics with those of the experimental model. If the difference is not minimal, the numerical model could be updated to match the experimental results.

- **Step 3 - Case studies: Identification of the reference frequencies:** Using the numerical model from step 2, determine the natural frequencies of the free-free beam in the following cases: single damage beam and double damages beam (reference frequencies of the case studies).

- **Step 4 - Case studies: Results and discussions:** Using the numerical model from step 2 and the reference frequencies from step 3, define the numerical model closest to the damage model using optimization algorithms. If an equivalent numerical model is found, compare the damage location and damage index of the numerical model with the reference cases to verify the accuracy of the damage identification approach.

- **Step 5 - Identification of damage base on experimental data:** Conduct experiments to determine the natural frequencies of single damage beam and double damages beams. Use the numerical model based on experimental data to locate damage and compare with the experimental results.

3 Intact free-free beam experiment

In this study, a free-free beam with a length of 1000 mm and a rectangle cross-section of 70 mm width and 10 mm thickness is considered. The beam has free-free boundary conditions with the help of two thin filaments installed at 220 mm and 780 mm along its length. The beam material is steel with a density of 7820 kg/m3 and a Poisson's ratio of 0.2. The finite element model used in this study is based on these material properties. The vibration characteristics of the beam are measured using fifteen accelerometers, National Instruments equipment, and a laptop. These measurements are then converted from

the time domain to the frequency domain to determine the natural frequencies of this beam. This experiment was performed by Duong N et al. [61], and the layout of the test beam is shown in Fig. 1 and Fig. 2.

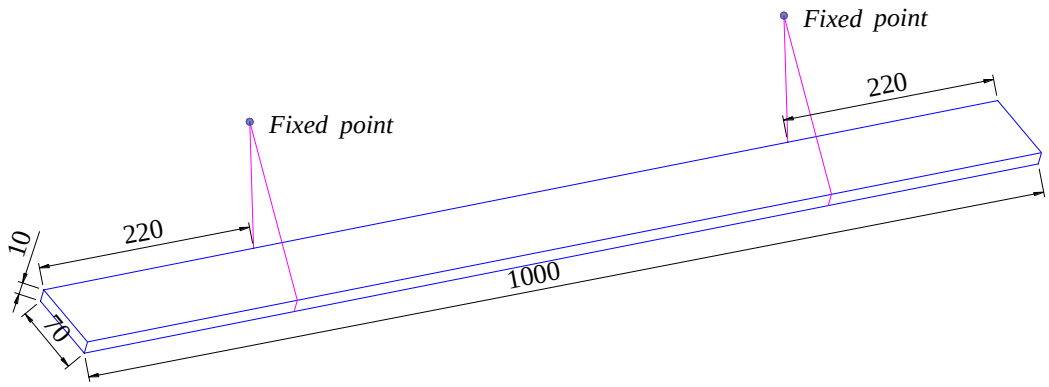

Fig. 1 - The layout of the test beam

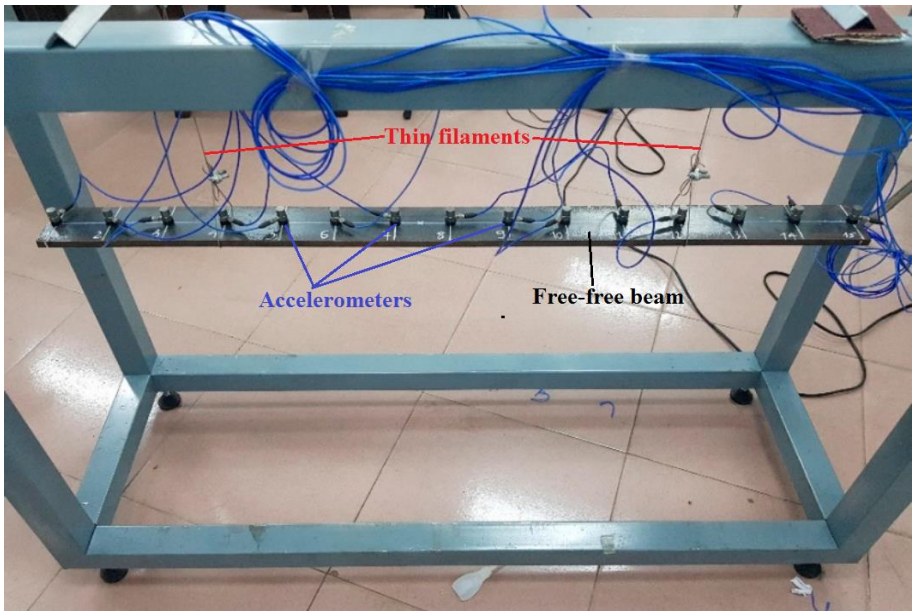

Fig. 2 – Experimental setup [61]

The experimental natural frequencies of the first five vertical bending modes of the intact beam were found to be 50.83 *Hz*, 140.40 *Hz*, 274.74 *Hz*, 456.94 *Hz*, and 678.90 *Hz* , [61]. These natural frequencies serve as a benchmark for comparison with the results from the numerical model to evaluate its accuracy.

4 Validation of numerical model

A finite element model of the test beam was created using Matlab's Partial Differential Equation Toolbox [62], with three-dimensional (3D) tetrahedral elements. The beam has dimensions of 1000 *mm* in length, 70 *mm* in width, and 10 *mm* in thickness, and is made of steel with an elastic modulus of 200 *GPa*, a Poisson's ratio of 0.3, and a mass density of 7820 kg/m^3. The impact of element size on natural frequencies was studied by varying the element size from 0.5 *m* to 0.01 *m*. The results of the first five vertical bending natural frequencies versus element sizes are presented in Fig. 3. It was found that that natural frequencies converge when the element size reaches 0.01 m, which was therefore selected as the maximum element size. Fig. 4 shows the meshed elements, and Fig. 5 shows the first five vertical bending natural frequencies and their corresponding mode shapes. The natural frequencies for modes 1 to 5 were found to be 50.878 *Hz*, 140.299 *Hz*, 275.173 *Hz*, 455.156 *Hz*, and 680.312 *Hz*, respectively.

Table 1 presents a comparison of the experimental and numerical results for the intact beam. The maximum error between two models was equal to 0.391%. This demonstrates the accuracy of the numerical model compared to the experimental model in this work.

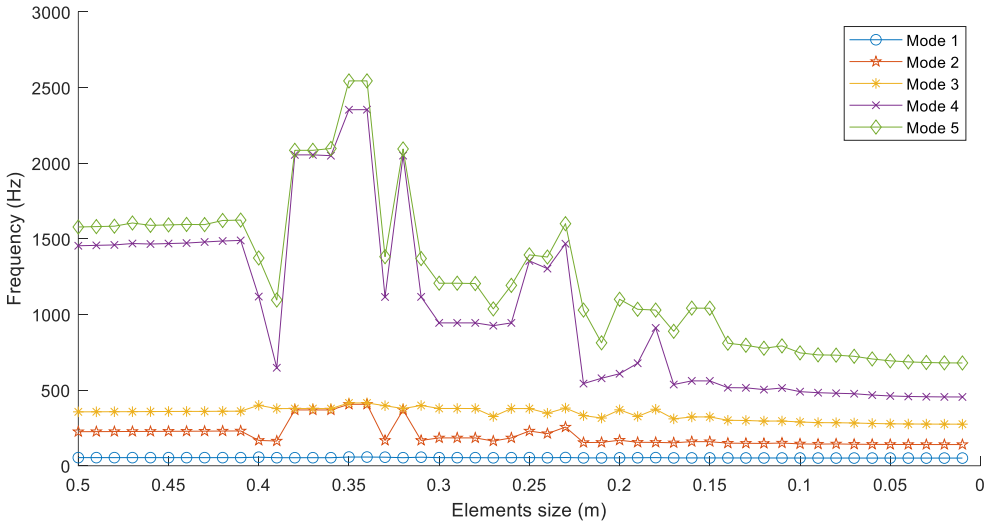

Fig. 3 – Natural frequencies vs. Element sizes (number of elements)

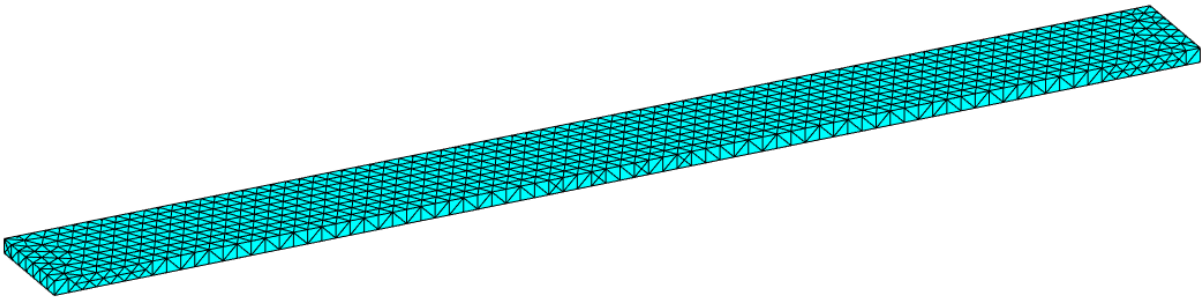

Fig. 4 – Beam mesh in Finite Element model (maximum elements size of 0.01 m)

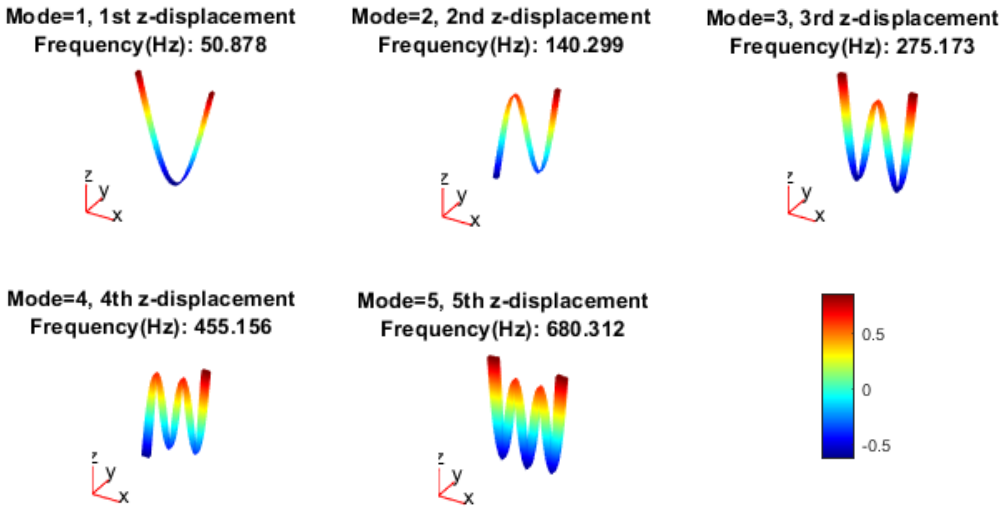

Fig. 5 – First five vertical bending frequencies and mode shapes of the test beam

Table 1 - Experimental and numerical natural frequencies of the intact beam.

Mode	Natural frequencies of the intact beam		
	Experimental	Numerical	Error (%)
1	50.83	50.878	0.094%
2	140.40	140.299	0.072%
3	274.74	275.173	0.158%
4	456.94	455.156	0.391%
5	678.90	680.312	0.208%

5 Case studies: Identification of the reference frequencies

5.1 Case study 1 - Single damage beam - symmetry - same damage index

In the first case study, the focus was on the symmetry analysis of the damage zone in the single damage beam cas. Four different damage cases were considered, each with a damage zone of 5x17.5 *mm*, equivalent to 25% damage index. The damage cases were named D11, D12, D13, and D14, and were located at ¼ length of the beam on the right side in the horizontal direction (D11), symmetrical along the longitudinal direction of the beam relative to D11 (D12), symmetrical along the transverse direction relative to D11 (D13), and symmetrical along the transverse direction relative to D13 (D14). The damage cases are described in Table 2 and shown in Fig. 6. The natural frequencies of the four cases, obtained from the numerical model, are listed in Table 3 as reference frequencies.

Table 2 - Symmetry single damage beam.

No	Damage case	Damage location	Damage index	Detail
1-1	D11	250 *mm*	25%	Reference case
1-2	D12	250 *mm*	25%	Symmetrical along the longitudinal direction of the beam relative to D11
1-3	D13	750 *mm*	25%	Symmetrical along the transverse direction relative to D11
1-4	D14	750 *mm*	25%	Symmetrical along the transverse direction relative to D13

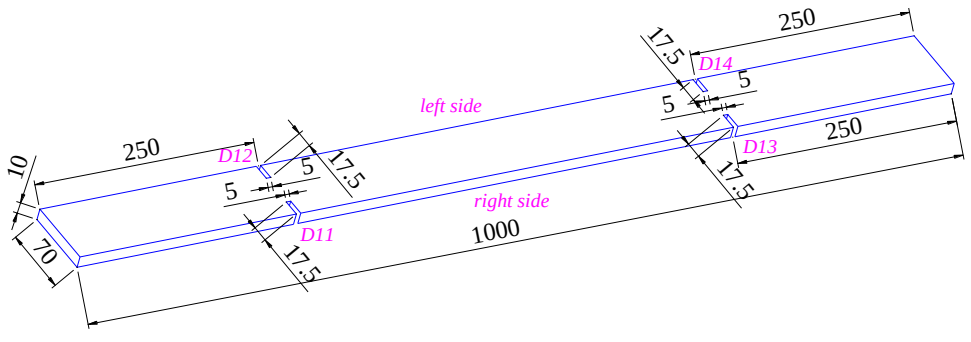

Fig. 6 - Symmetry single damage beam

5.2 Case study 2 - Single damage beam - same positions - different damage index

In the second case study, the focus was on the analysis of a single damage beam with two symmetrical damage zones in the transverse direction, located at 4/10 length of the beam. The damage zones had different damage indexes of 40%, 30%, 20%, and 10% (calculated based on the damage length and beam width). These damage cases are listed in Table 4 and depicted in Fig. 7. The numerical natural frequencies for these cases are listed in Table 5 as reference frequencies.

Table 3 - Numerical natural frequencies of case study 1 - Reference frequencies.

Mode	Reference frequencies			
	D11	D12	D13	D14
1	50.718	50.718	50.718	50.718
2	139.209	139.209	139.209	139.209
3	273.400	273.400	273.400	273.400
4	454.609	454.609	454.609	454.609
5	679.603	679.603	679.603	679.603

Table 4 - Single damage beam with different damage index.

No	Damage case	Damage location	Damage index	Detail
2-1	D21	400 mm	40%	Damage index of 40%
2-2	D22	400 mm	30%	Damage index of 30%
2-3	D23	400 mm	20%	Damage index of 20%
2-4	D24	400 mm	10%	Damage index of 10%

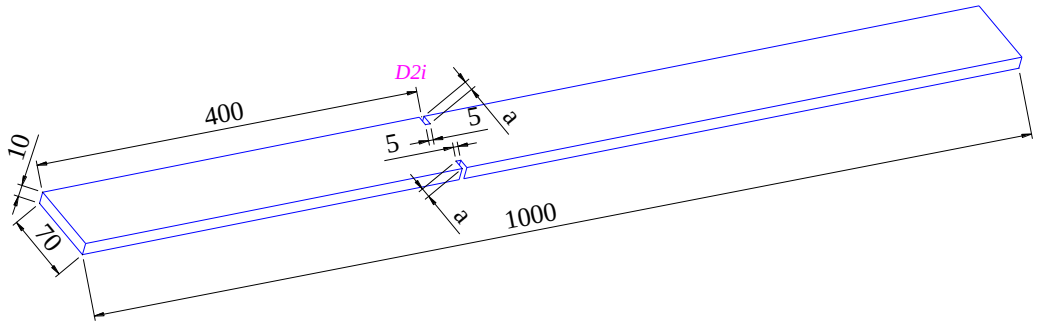

Fig. 7 - Single damage cases with different damage index

Table 5 - Numerical natural frequencies of case study 2 - Reference frequencies.

Mode	Reference frequencies			
	D21	D22	D23	D24
1	50.258	50.524	50.730	50.831
2	139.500	139.858	140.129	140.257
3	274.589	274.889	275.123	275.211
4	450.946	452.861	454.400	455.081
5	679.895	680.356	680.694	680.723

5.3 Case study 3 - Free-free beam with double damage zones

The third case study focused on the effects of having double damage zones, with each zone having two damages, one on the left side of the beam and one on the right side. Table 6 shows the four different cases of double damage zones, with varying damage locations and indexes. The cases include having the same minor damage index, having the same major damage index, having damages located fat apart from each other, and having damages close together. Table 7 presents the numerical natural frequencies of the third case study, referred as reference frequencies. These results can help understand the impact of multiple damage zones on the natural frequencies of a free-free beam and can be useful in the diagnosis of damages in structures.

Table 6 - Double damage beam.

No	Damage case	Damage location	Damage index	Detail
3-1	D31	200 mm	10%	Same minor damage index
		500 mm	10%	
3-2	D32	200 mm	30%	Same major damage index
		500 mm	30%	
3-3	D33	250 mm	20%	Long distance
		500 mm	25%	
3-4	D34	450 mm	20%	Close distance
		500 mm	25%	

Table 7 - Numerical natural frequencies of case study 3 - Reference frequencies.

Mode	Reference frequencies			
	D31	D32	D33	D34
1	50.814	50.396	50.553	50.432
2	140.216	139.604	139.918	140.24
3	274.841	271.806	273.657	273.811
4	455.075	452.84	455.014	454.769
5	680.302	675.812	678.141	677.688

6 Case studies: Results and discussions

The damage location and the damage index of the free-free beam can be determined using optimization algorithms based on the reference frequency data as mentioned previously. Some of the optimization algorithms can be mentioned as: the Particle Swarm Optimization (PSO), Genetic Algorithm (GA), Cuckoo algorithm [63-66]. In this study, the PSO algorithm was applied to solve the problem. The Particle Swarm Optimization algorithm was developed in 1985 by Kennedy, J., and R. Eberhart [64, 65], inspired by the idea that a group of birds or fish could move more effectively by sharing information about their foraging. The PSO algorithm generates the initial position of particles within a constrained range as a random uniform variable, calculates the objective function value, and determines the best position for each particle and the best position for the entire group of particles. Each particle's velocity and position are then updated based on these two best positions, and the process is repeated until a termination condition is met, usually when the objective function value is reached or after a certain number of iterations. An illustration of the PSO's workflow is shown in Fig. 8. By updating the numerical model with the damage location and damage index as the parameters to be optimized, the optimization algorithm was able to determine the damage characteristics of the beam based on the reference frequencies. The natural frequencies are considered to develop the objective functions as follows:

$$f_{obj} = \sum_{i=1}^{n} \left[100 \times \frac{f_{Ref} - f_{FE}}{f_{Ref}} \right]^2 \tag{1}$$

where:

- f_{FE}, f_{Ref} are the natural frequencies of the updating model and reference (experimental) frequencies, respectively.
- n is number of considered modes.

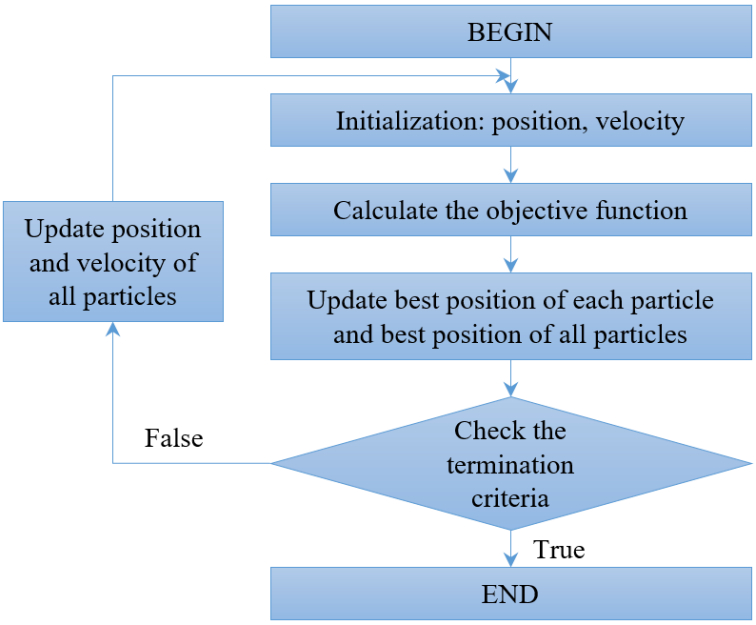

Fig. 8 – Block diagram of PSO algorithm

Fig. 9 - Damage location of case study 1 in the optimization algorithms

6.1 Case study 1 - Single damage beam - symmetry - same damage index

By updating the numerical model with the damage location and damage index as the parameters to be optimized, the optimization algorithm was able to determine the damage characteristics of the beam based on the reference frequencies in Table 3. Fig. 9 and Table 8 show the results of the model updating process, including the damage index and damage location. This demonstrates the high accuracy of the numerical model updating approach in detecting the damage location and determining the damage index. The small error values (less than 0.2% for the damage location and less than 1.6% for the damage index) indicate that the numerical model is able to precisely identify both the location and extent of the damage.

In the figure below, the damage locations are shown as coordinates represented by cyan and yellow dots, where the distance from the cyan dot to the left side of the plate represents the damage length (and thus the damage index), and the distance from the yellow dot to the right side of the plate represents the damage length (damage index). The red circles

correspond to the four reference damage cases D11, D12, D13, and D14, and the blue multiplication signs indicate the damage found after model updating.

Table 8 - Damage location and damage index of case study 1: Optimization algorithm vs. References.

No	Damage case	References		Optimization algorithm		Error (%)	
		Damage location (mm)	Damage length (mm) (25% damage index)	Damage location (mm)	Damage length (mm)	Damage location	Damage length
1-1	D11	250	17.5	250.05	17.62	0.019%	0.688%
1-2	D12	250	17.5	250.33	17.44	0.130%	0.367%
1-3	D13	750	17.5	749.50	17.32	0.066%	1.030%
1-4	D14	750	17.5	749.27	17.23	0.097%	1.518%

The results shown in Fig. 9, involving radial or axial symmetrical damages, are typical of many of the results of the model updating. Since the reference frequencies for all four cases in Table 3 are identical, it makes sense that the model updating results could be one of the four damage locations shown in Fig. 9. The results indicate that the density of damages found in the zones surrounding the hypothetical damage locations (represented by the red circles) is much higher compared to other zones of the beam. This demonstrates that the optimazation algorithm gradually converges to these hypothetical points (red circles) and provides accurate results. In Fig. 9, the coordinates of points to be close to the coordinates of the hypothetical points, the low number of green points on the right and yellow points on the left suggest that the damage index can be easier to converge than the damage location. Additionally, for each case in Fig. 9, the yellow points tend to be axially symmetrical with the cyan points, while they are all not symmetrical about the mid-beam transverse axis. This demonstrates that the optimization algorithms are effective in finding the damage locations.

6.2 Case study 2 - Single damage beam - same positions - different damage index

The numerical model, after being updated based on the reference frequencies given in Table 5, was successful in determining the location and index of damage for the case study 2. The results for case D21 are shown in Fig. 9, the other cases have similar results and are summarized in Table 9. Each of the four cases (D21, D22, D23 and D24) is run three times to check the stability of the results. For the case study 2, the damage zones are symmetrical in the transverse direction, so the yellow points are also symmetrical to the cyan points.

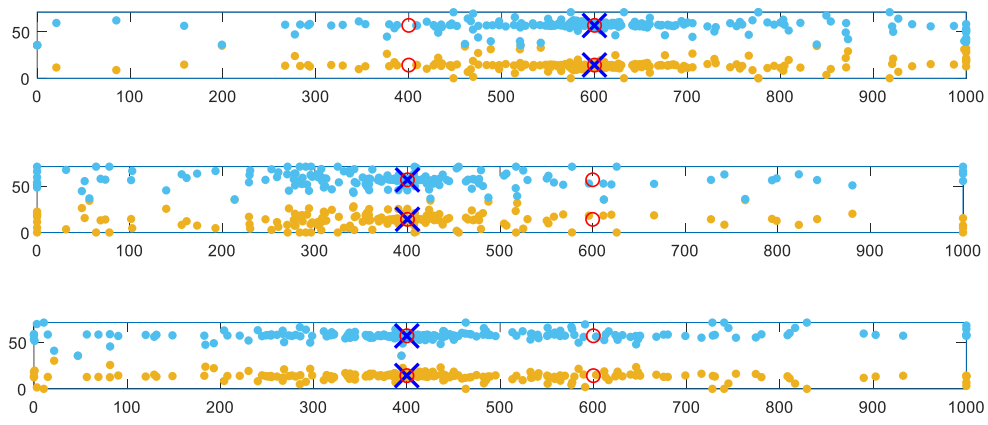

Fig. 10 - Damage location of case D21 in the optimization algorithms

Similar to case study 1, the damage locations are discovered symmetrically along the axis at mid-beam (0.4 *m* and 0.6 *m* in this instance). The results in Table 9 showed that the damage location errors were found to be less than 0.6% and the damage index errors were less than 2%. This suggests that the method used to obtain the natural frequencies in this case study

is consistent and reliable, as the results obtained from multiple runs are similar and do not vary significantly. The error of the damage location is inversely proportional to the damage index, meaning that larger damage index values result in smaller error values for the damage location. For example, in the case of D21 with a damage index of 40%, the error of the damage location was found to be less than 0.03%. However, for the case of D24 with a damage index of 10%, the error of the damage location was nearly 1.8%. The results demonstrate the effectiveness of the numerical model updating approach for determining the location and index of damage in case study 2.

Table 9 - Damage location and damage index of case study 2: Optimization algorithm vs. References.

No	Damage case		References		Optimization algorithm		Error (%)	
			Damage location (mm)	Damage index	Damage location (mm)	Damage index	Damage location	Damage index
2-1	D21	1st time	600	40%	599.91	40.38%	0.015%	0.959%
		2nd time	400	40%	400.02	40.35%	0.006%	0.872%
		3rd time	400	40%	399.90	40.30%	0.025%	0.750%
2-2	D22	1st time	600	30%	599.77	30.00%	0.038%	0.013%
		2nd time	600	30%	599.93	30.11%	0.012%	0.355%
		3rd time	600	30%	599.83	30.10%	0.029%	0.342%
2-3	D23	1st time	600	20%	600.10	20.02%	0.016%	0.119%
		2nd time	400	20%	400.45	19.61%	0.112%	1.934%
		3rd time	600	20%	599.55	19.73%	0.075%	1.368%
2-4	D24	1st time	600	10%	599.76	9.87%	0.040%	1.250%
		2nd time	600	10%	601.25	9.82%	0.208%	1.778%
		3rd time	600	10%	603.12	9.86%	0.520%	1.407%

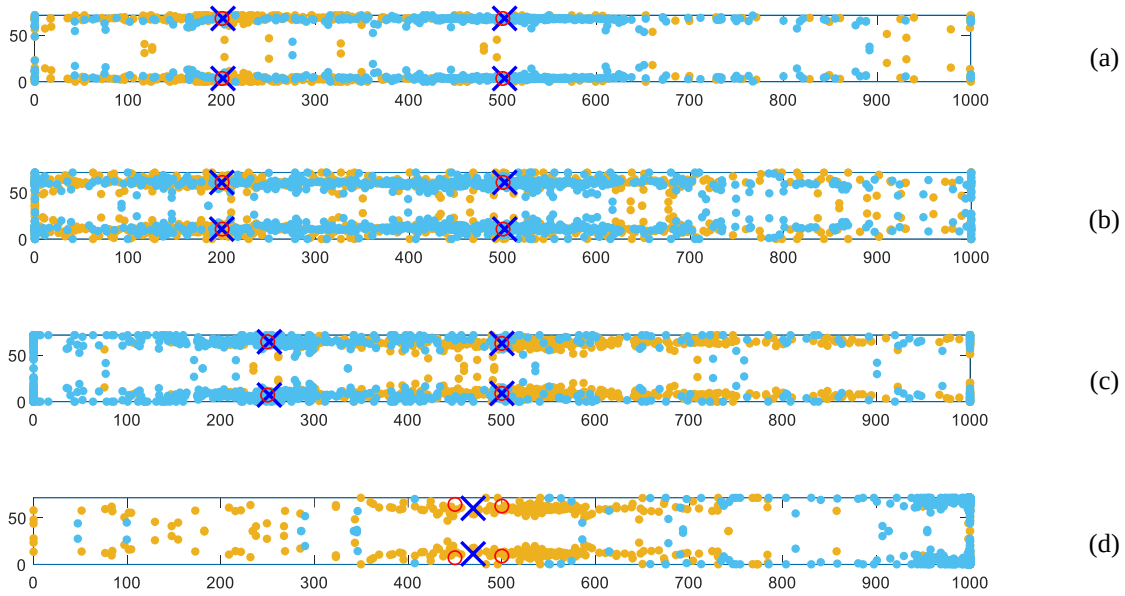

Fig. 11 – Damage location of case study 3 in the optimization algorithms: (a) D31 case, (b) D32 case, (c) D33 case, and (d) D34 case

6.3 Case study 3 - Free-free beam with double damage zones

Similar to the two case studies mentioned previously, the numerical model, after being updated with the optimal algorithm based on the reference frequencies, will be able to determine the damage location as well as the damage index in the following cases: two damages at two different locations with the same minor damage index, two damages at two different locations with the same major damage index, two damages that are far apart, and two damages that are close together. To verify the stability of the results from the model updating method, each case was run three times, and the results are summarized in Table 10. The results of the typical runs of each case are shown in Fig. 11. Cyan and yellow dots represent first and second damage locations (if any). The results in Fig. 11 and Table 10 have been rearranged to correspond with the reference cases when considering the axial symmetry (mentioned in the previous sections).

The obtained results indicate that the damage finding method based on the reference frequencies provides quite accurate results for the case with the same minor damage index, the case with the same major damage index, and the case with a long distance between damages. The result is very close to the reference cases. However, for the case with damages close together (D34), this method gives incorrect results in three runs. Two of them indicate one damage that locate in the middle of two damages in the reference case corresponding, and one indicates two damages that are not very close to the reference case. This can be explained because the optimization algorithm used did not find a truly optimal solution.

Table 10 - Damage location and damage index of case study 3: Optimization algorithm vs. References.

No	Damage case		References				Optimization algorithm			
			1st damage		2nd damage		1st damage		2nd damage	
			Damage location (mm)	Damage index	Damage location (mm)	Damage index	Damage location (mm)	Damage index	Damage location (mm)	Damage index
3-1	D31	1st time (*)	201	10%	502	10%	200	10%	500	10%
		2nd time	199	10%	497	10%	200	10%	500	10%
		3rd time	200	10%	496	10%	200	10%	500	10%
3-2	D32	1st time (*)	200	30%	502	30%	200	30%	500	30%
		2nd time	200	30%	502	30%	200	30%	500	30%
		3rd time	200	30%	501	30%	200	30%	500	30%
3-3	D33	1st time (*)	252	20%	500	25%	250	20%	500	25%
		2nd time	250	20%	497	25%	250	20%	500	25%
		3rd time	250	20%	504	25%	250	20%	500	25%
3-4	D34	1st time (*)	469	32%			450	20%	500	25%
		2nd time	453	5%	469	31%	450	20%	500	25%
		3rd time	468	31%			450	20%	500	25%

Note: (*) is the case *shown in Fig. 11.*

7 Identification of damage base on experimental data

7.1 Experimental results for the damage beam

To validate the damage detection approach, two scenarios were performed in the experiment described in Section 3 [61]:

- *Scenario 1*: A damage was introduced at position 325 *mm* with a length of 12.5 *mm*, width of 0.5 *mm*, and depth of 10 *mm*. The stiffness of the damage zone was equal to 82.14% of the intact beam's stiffness.

- *Scenario 2*: Two damage zones were introduced at the same position 325 *mm*. The first damage had a length of 12.5 *mm*, width of 0.5 *mm*, and depth of 10 *mm* (the same as the Scenario 1) on the left side of the beam. The second

damage had a length of 13.3 *mm*, width of 0.5 *mm*, and depth of 10 *mm*, on the right side of the beam. The total remaining stiffness of the two damage zones was equal to 63.14% of the intact beam's stiffness.

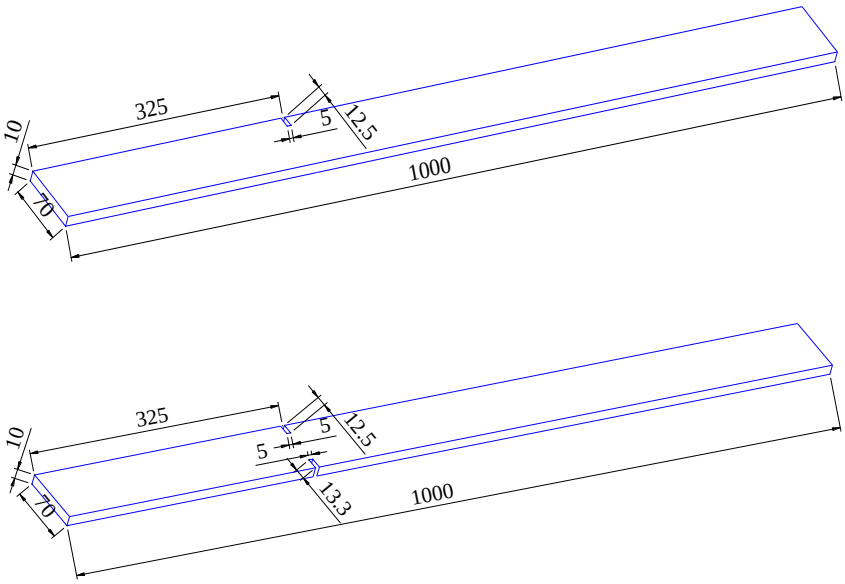

Fig. 12 - The layout of the damage beam (a) scenario 1, (b) scenario 2

The damage in the scenarios 1 is illustrated in Fig. 12a while the damage in the scenarios 2 is illustrated in Fig. 12b and Fig. 13. Table 11 shows the experimental natural frequencies of the first five vertical bending modes of the single damage beam and the double damages beam [61]. These natural frequencies were used to update the numerical model and locate the damage.

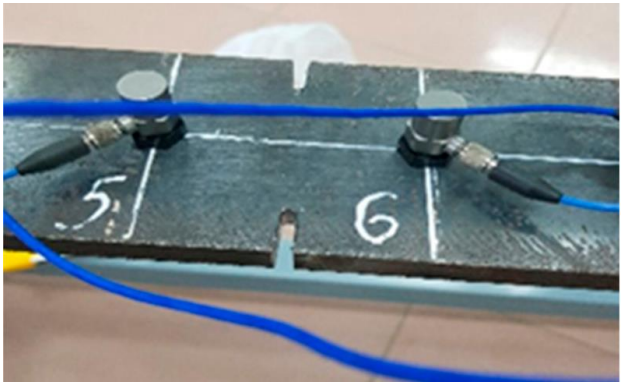

Fig. 13 - The cutting places in the damaged beam [61]

Table 11 – Experimental natural frequencies of two scenarios.

Mode	Experimental natural frequencies	
	Scenario 1	Scenario 2
1	50.65	50.36
2	139.69	138.64
3	273.77	273.53
4	456.38	454.60
5	675.99	672.58

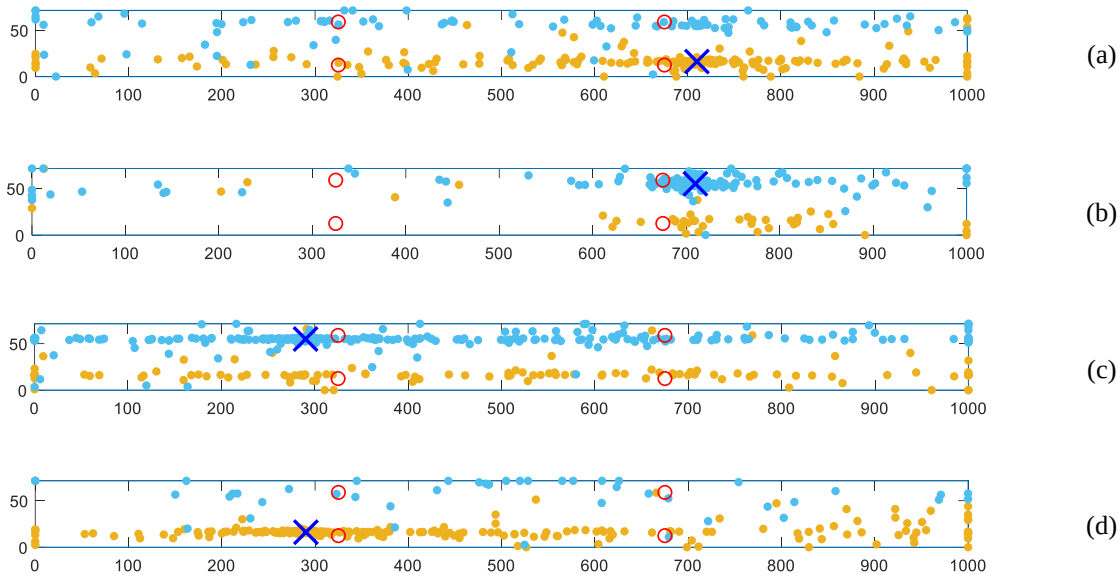

Fig. 14 - Damage location of scenario 1

7.2 Determination of damage location

Based on the experimental natural frequencies of the first five bending modes in Table 11, the updated numerical model was able to detect damages and determine their characterics. The results of four runs for each scenario are shown in Fig. 14, Fig. 15, Table 12 , and Table 13. For scenario 1, even though the damage only occurs on the left side at a position 325 *mm* from the end of the beam, due to its symmetrical nature, the damage location is shown at all four positions, as indicated by the red circles in Fig. 14. The damage position in the numerical model also appeared at four similar symmetry positions, indicated by the blue multiplication signs in Fig. 14. The presentation of the results for Scenario 2 is done in a similar manner, as shown in Fig. 15.

Table 12 - Damage location and damage index of scenario 1.

No	Experimental			Optimization algorithm		
	Damage location (mm)	Damage length (mm)	Side	Damage location (mm)	Damage length (mm)	Side
1	325	12.5	left	710	16.28	right
2	325	12.5	left	710	16.35	left
3	325	12.5	left	290	16.43	left
4	325	12.5	left	290	16.19	right

Table 13 – Damage location and damage index of scenario 2.

No	Experimental						Optimization algorithm					
	1st damage			2nd damage			1st damage			2nd damage		
	Damage location (mm)	Damage length (mm)	Side	Damage location (mm)	Damage length (mm)	Side	Damage location (mm)	Damage length (mm)	Side	Damage location (mm)	Damage length (mm)	Side
1	325	12.5	right	325	13.3	left	697	23.70	right	697	1.35	left
2	325	12.5	right	325	13.3	left	302	1.56	right	302	23.77	left
3	325	12.5	right	325	13.3	left	697	23.54	right	697	2.06	left
4	325	12.5	right	325	13.3	left	698	23.76	right	698	1.58	left

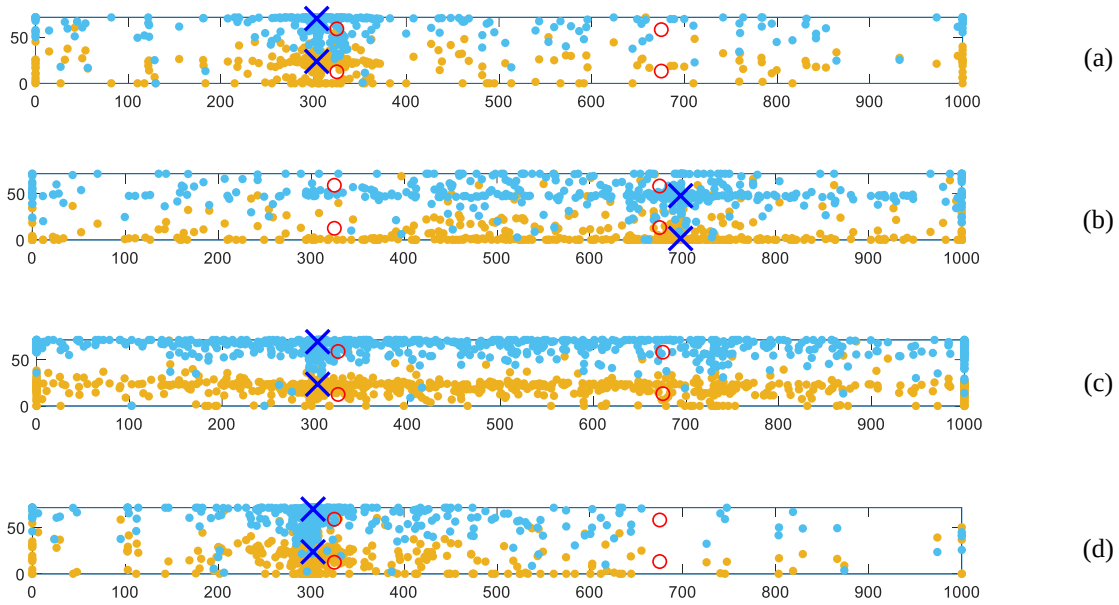

Fig. 15 - Damage location of scenario 2

The high concentration of cyan and yellow points near the numerical model's results indicates that model is converging well to the final results. However, the location of the damage was found to to be different from the location in the experiment, with a distance of 35 *mm* of the scenario 1 and with a distance of 22-23 *mm* of the scenario 2 for all four runs. In term of the entire length of the beam, this error amounts to 35 *mm*/1000 *mm* = 3.5% for the first scenario and 23 *mm*/1000 *mm* = 2.3% for the second scenario. This error is much larger than the results shown in Table 8, Table 9, and Table 10. The cause of this error comes from the determination of the natural frequencies in the experiment, as each measurement yields a different set of frequency results, although they are very close to each other. The numerical model's input frequency values are also found to be more sensitive compared to the results of finding the damage location and damage index. The error may also be due to incorrect measurement of the damage dimension in the test beam. However, this error is acceptable in practice. For example, in a structure with a length of 40 *m*, the damage position as determined by the numerical model would differ by approximately 3.5% x 40 *m* = 1.4 *m* from the actual damage position. As a result, the damage determination method based on the natural frequency will show the relative position of the damage on the beam, after which the engineers can inspect the damage more closely.

8 Conclusion

This paper presents a numerical model updating method based on the reference frequencies to determine the location and characteristics of damage in a free-free beam. The method involves updating the numerical model using experimental natural frequencies of the first five bending modes of the beam. The model is updated using an optimization algorithm, and the results are verified through comparison with reference cases and experimental results. The results show that the method provides accurate results for the single damage beam, and with minor or major damage, or damages that are far apart for the double damage beam. However, for cases with damages close together, the results are incorrect and further optimization is required. The experimental results validate the effectiveness of the model updating method, although with some error in the determination of the damage location. Nevertheless, the method provides an acceptable level of accuracy in practice and can be used to determine the relative position of damage on a beam for further inspection.

REFERENCES

[1]- S. Fotouhi, F. Pashmforoush, M. Bodaghi, M. Fotouhi, Autonomous damage recognition in visual inspection of laminated composite structures using deep learning. Composite Structures, 268 (2021) 113960. doi:10.1016/j.compstruct.2021.113960.

[2]- A.C. Estes, D.M. Frangopol, S.D. Foltz, Updating reliability of steel miter gates on locks and dams using visual

inspection results. Engineering Structures, 26(3) (2004) 319-333. doi:10.1016/j.engstruct.2003.10.007.
[3]- J.W. Schoonahd, J.D. Gould, L.A. Miller, Studies of Visual Inspection. Ergonomics, 16(4) (1973) 365-379. doi:10.1080/00140137308924528.
[4]- X. Jiang, A.K. Gramopadhye *, B.J. Melloy, Theoretical issues in the design of visual inspection systems. Theoretical Issues in Ergonomics Science, 5(3) (2004) 232-247. doi:10.1080/1463922021000050005.
[5]- X. Cheng, G. Ma, Z. Wu, H. Zu, X. Hu, Automatic defect depth estimation for ultrasonic testing in carbon fiber reinforced composites using deep learning. NDT & E International, 135 (2023) 102804. doi:10.1016/j.ndteint.2023.102804.
[6]- T. Arakawa, S. Hirose, T. Senda, The detection of weld cracks using ultrasonic testing. NDT International, 18(1) (1985) 9-16. doi:10.1016/0308-9126(85)90037-9.
[7]- X. Chen, Z. Ye, J.Y. Xia, J.X. Wang, B.H. Ji, Double-Probe Ultrasonic Detection Method for Cracks in Steel Structure. Applied Sciences, 10(23) (2020) 8436. doi:doi:10.3390/app10238436.
[8]- P.L. Liu, L.C. Lin, Y.Y. Hsu, C.Y. Yeh, P.L. Yeh, Recognition of rebars and cracks based on impact-echo phase analysis. Construction and Building Materials, 142 (2017) 1-6. doi:10.1016/j.conbuildmat.2017.02.102.
[9]- Y.-x. Yang, W.-h. Chai, D.-c. Liu, W.-d. Zhang, J.-c. Lu, Z.-k. Yang, An Impact-Echo Experimental Approach for Detecting Concrete Structural Faults. Advances in Civil Engineering, 2021 (2021) 8141015. doi:10.1155/2021/8141015.
[10]- S. Dorafshan, H. Azari, Evaluation of bridge decks with overlays using impact echo, a deep learning approach. Automation in Construction, 113 (2020) 103133. doi:10.1016/j.autcon.2020.103133.
[11]- E. Çam, S. Orhan, M. Lüy, An analysis of cracked beam structure using impact echo method. NDT & E International, 38(5) (2005) 368-373. doi:10.1016/j.ndteint.2004.10.009.
[12]- A. Koko, S. Singh, S. Barhli, T. Connolley, N.T. Vo, T. Wigger, D. Liu, Y. Fu, J. Réthoré, J. Lechambre, J.Y. Buffiere, T.J. Marrow, 3-Dimensional analysis of fatigue crack fields and crack growth by in situ synchrotron X-ray tomography. International Journal of Fatigue, 170 (2023) 107541. doi:10.1016/j.ijfatigue.2023.107541.
[13]- N. Limodin, J. Réthoré, J.-Y. Buffière, F. Hild, S. Roux, W. Ludwig, J. Rannou, A. Gravouil, Influence of closure on the 3D propagation of fatigue cracks in a nodular cast iron investigated by X-ray tomography and 3D volume correlation. Acta Materialia, 58(8) (2010) 2957-2967. doi:10.1016/j.actamat.2010.01.024.
[14]- R. Helwing, D. Hülsbusch, F. Walther, Deep learning method for analysis and segmentation of fatigue damage in X-ray computed tomography data for fiber-reinforced polymers. Composites Science and Technology, 230 (2022) 109781. doi:10.1016/j.compscitech.2022.109781.
[15]- B. Yu, R. Bradley, C. Soutis, P. Withers, A comparison of different approaches for imaging cracks in composites by X-ray microtomography. Philosophical Transactions of the Royal Society A: Mathematical, Physical and Engineering Sciences, 374 (2016) 20160037. doi:10.1098/rsta.2016.0037.
[16]- C. Kim, S. Hwang, H. Sohn, Weld crack detection and quantification using laser thermography, mask R-CNN, and CycleGAN. Automation in Construction, 143 (2022) 104568. doi:10.1016/j.autcon.2022.104568.
[17]- E. Ichi, S. Dorafshan, Effectiveness of infrared thermography for delamination detection in reinforced concrete bridge decks. Automation in Construction, 142 (2022) 104523. doi:10.1016/j.autcon.2022.104523.
[18]- L. Solovyov, A. Solovyov, V. Fedorenko, Thermal Method for Detecting Fatigue Cracks in Welded Steel Bridges Under Random Loads. Transportation Research Procedia, 61 (2022) 588-593. doi:10.1016/j.trpro.2022.01.095.
[19]- M. Eskandari Torbaghan, W. Li, N. Metje, M. Burrow, D.N. Chapman, C.D.F. Rogers, Automated detection of cracks in roads using ground penetrating radar. Journal of Applied Geophysics, 179 (2020) 104118. doi:10.1016/j.jappgeo.2020.104118.
[20]- S. Li, X. Gu, X. Xu, D. Xu, T. Zhang, Z. Liu, Q. Dong, Detection of concealed cracks from ground penetrating radar images based on deep learning algorithm. Construction and Building Materials, 273 (2021) 121949. doi:10.1016/j.conbuildmat.2020.121949.
[21]- T. Chan, D. Thambiratnam, Structural health monitoring in Australia. 1-229, 2014.
[22]- C. Farrar, K. Worden, Structural Health Monitoring A Machine Learning Perspective. 2013.
[23]- D. Balageas, C.P. Fritzen, A. Güemes, Structural Health Monitoring. Wiley, 2010.
[24]- R. Yan, X. Chen, S.C. Mukhopadhyay, Structural Health Monitoring: An Advanced Signal Processing Perspective. 2017.
[25]- S. Doebling, C. Farrar, M. Prime, A Summary Review of Vibration-Based Damage Identification Methods. The Shock and Vibration Digest, 30 (1998) 91-105. doi:10.1177/058310249803000201.

[26]- C. Farrar, F. Hemez, D. Shunk, D. Stinemates, B. Nadler, A Review of Structural Health Monitoring Literature: 1996–2001. 2004.
[27]- W. Fan, P. Qiao, Vibration-based Damage Identification Methods: A Review and Comparative Study. Structural Health Monitoring-an International Journal - STRUCT HEALTH MONIT, 9 (2010). doi:10.1177/1475921710365419.
[28]- T. Bui-Tien, Q.T. Nguyen, L.V. Ho, A hybrid heuristic optimization algorithm PSOGSA coupled with a hybrid objective function using ECOMAC and frequency in damage detection. Journal of Materials and Engineering Structures, 8(1) (2021) 15.
[29]- W. Zhang, J. Li, H. Hao, H. Ma, Damage detection in bridge structures under moving loads with phase trajectory change of multi-type vibration measurements. Mechanical Systems and Signal Processing, 87 (2017) 410-425. doi:10.1016/j.ymssp.2016.10.035.
[30]- W.R. Wickramasinghe, D.P. Thambiratnam, T.H.T. Chan, T. Nguyen, Vibration characteristics and damage detection in a suspension bridge. Journal of Sound and Vibration, 375 (2016) 254-274. doi:10.1016/j.jsv.2016.04.025.
[31]- S. Baba, J. Kondoh, Damage evaluation of fixed beams at both ends for bridge health monitoring using a combination of a vibration sensor and a surface acoustic wave device. Engineering Structures, 262 (2022) 114323. doi:10.1016/j.engstruct.2022.114323.
[32]- S.M. Seyedpoor, O. Yazdanpanah, An efficient indicator for structural damage localization using the change of strain energy based on static noisy data. Applied Mathematical Modelling, 38(9) (2014) 2661-2672. doi:10.1016/j.apm.2013.10.072.
[33]- D.H. Nguyen, Q.B. Nguyen, T. Bui-Tien, G. De Roeck, M. Abdel Wahab, Damage detection in girder bridges using modal curvatures gapped smoothing method and Convolutional Neural Network: Application to Bo Nghi bridge. Theoretical and Applied Fracture Mechanics, 109 (2020) 102728. doi:10.1016/j.tafmec.2020.102728.
[34]- H. Wan, L. Gao, Z. Yuan, H. Qu, Q. Sun, H. Cheng, R. Wang, A novel transformer model for surface damage detection and cognition of concrete bridges. Expert Systems with Applications, 213 (2023) 119019. doi:10.1016/j.eswa.2022.119019.
[35]- M. Gordan, H.A. Razak, Z. Ismail, K. Ghaedi, Z.X. Tan, H.H. Ghayeb, A hybrid ANN-based imperial competitive algorithm methodology for structural damage identification of slab-on-girder bridge using data mining. Applied Soft Computing, 88 (2020) 106013. doi:10.1016/j.asoc.2019.106013.
[36]- L. Chen, W. Chen, L. Wang, C. Zhai, X. Hu, L. Sun, Y. Tian, X. Huang, L. Jiang, Convolutional neural networks (CNNs)-based multi-category damage detection and recognition of high-speed rail (HSR) reinforced concrete (RC) bridges using test images. Engineering Structures, 276 (2023) 115306. doi:10.1016/j.engstruct.2022.115306.
[37]- A. Kamariotis, E. Chatzi, D. Straub, A framework for quantifying the value of vibration-based structural health monitoring. Mechanical Systems and Signal Processing, 184 (2023) 109708. doi:10.1016/j.ymssp.2022.109708.
[38]- H. Nguyen-Tran, T. Bui-Tien, M.A. Wahab, D. Bui-Ngoc, Damage detection in structural health monitoring using combination of deep neural networks. Journal of Materials and Engineering Structures, 7(4) (2020) 8.
[39]- H. Nahvi, M. Jabbari, Crack detection in beams using experimental modal data and finite element model. International Journal of Mechanical Sciences, 47(10) (2005) 1477-1497. doi:10.1016/j.ijmecsci.2005.06.008.
[40]- D. Mironovs, S. Ručevskis, K. Dzelzītis, Prospects of Structural Damage Identification Using Modal Analysis and Anomaly Detection. Procedia Structural Integrity, 37 (2022) 410-416. doi:10.1016/j.prostr.2022.01.103.
[41]- M. Civera, L. Sibille, L. Zanotti Fragonara, R. Ceravolo, A DBSCAN-based automated operational modal analysis algorithm for bridge monitoring. Measurement, 208 (2023) 112451. doi:10.1016/j.measurement.2023.112451.
[42]- C. Rinaldi, J. Ciambella, V. Gattulli, Image-based operational modal analysis and damage detection validated in an instrumented small-scale steel frame structure. Mechanical Systems and Signal Processing, 168 (2022) 108640. doi:10.1016/j.ymssp.2021.108640.
[43]- S. Cao, H. Nian, J. Yan, Z. Lu, C. Xu, Modal analysis and damage localization in plate-type structures via TDD and PE methods based on the data of an integrated highspeed camera system. Mechanical Systems and Signal Processing, 178 (2022) 109309. doi:10.1016/j.ymssp.2022.109309.
[44]- N.T.C. Nguyen, M.Q. Tran, H. S. Sousa, T.V. Ngo, J. C. Matos, Damage detection of structural based on indirect vibration measurement results combined with Artificial Neural Network. Journal of Materials and Engineering Structures, 9(4) (2022) 8.
[45]- K.D. Dang, N.H. Nguyen, S. Lee, V.H. Luong, T.A. Le, Q.X. Lieu, A novel model order reduction-based two-stage

damage detection paradigm for trusses using time–history acceleration. Advances in Engineering Software, 176 (2023) 103374. doi:10.1016/j.advengsoft.2022.103374.

[46]- J. Cao, Z. Zhou, Y. Liu, Damage localization for prefabricated bridges group using the area-ratio of the strain time-history curve. Measurement, 198 (2022) 111172. doi:10.1016/j.measurement.2022.111172.

[47]- B. Chomette, Nonlinear multiple breathing cracks detection using direct zeros estimation of higher-order frequency response function. Communications in Nonlinear Science and Numerical Simulation, 89 (2020) 105330. doi:10.1016/j.cnsns.2020.105330.

[48]- Z.K. Peng, Z.Q. Lang, S.A. Billings, Crack detection using nonlinear output frequency response functions. Journal of Sound and Vibration, 301(3) (2007) 777-788. doi:10.1016/j.jsv.2006.10.039.

[49]- A.C. Altunışık, F.Y. Okur, V. Kahya, Automated model updating of multiple cracked cantilever beams for damage detection. Journal of Constructional Steel Research, 138 (2017) 499-512. doi:10.1016/j.jcsr.2017.08.006.

[50]- A.C. Altunışık, F.Y. Okur, V. Kahya, Modal parameter identification and vibration based damage detection of a multiple cracked cantilever beam. Engineering Failure Analysis, 79 (2017) 154-170. doi:10.1016/j.engfailanal.2017.04.026.

[51]- F.E. Gunawan, T.H. Nhan, M. Asrol, Y. Kanto, I. Kamil, Sutikno, A New Damage Index for Structural Health Monitoring: A Comparison of Time and Frequency Domains. Procedia Computer Science, 179 (2021) 930-935. doi:10.1016/j.procs.2021.01.082.

[52]- A. Maghsoodi, A. Ghadami, H.R. Mirdamadi, Multiple-crack damage detection in multi-step beams by a novel local flexibility-based damage index. Journal of Sound and Vibration, 332(2) (2013) 294-305. doi:10.1016/j.jsv.2012.09.002.

[53]- N. Duong, T. Bui, G. De Roeck, M. Abdel Wahab, Damage detection in Ca Non Bridge using transmissibility and artificial neural networks. Structural Engineering and Mechanics, 71(1) (2019) 175-183. doi:10.12989/sem.2019.71.2.175.

[54]- S. Khatir, D. Boutchicha, C. Le Thanh, H. Tran-Ngoc, T.N. Nguyen, M. Abdel-Wahab, Improved ANN technique combined with Jaya algorithm for crack identification in plates using XIGA and experimental analysis. Theoretical and Applied Fracture Mechanics, 107 (2020) 102554. doi:10.1016/j.tafmec.2020.102554.

[55]- L. Nguyen, H. Tran, S. Khatir, L. Thang, Q. Huu-Nguyen, G. De Roeck, T. Bui Tien, M. Wahab, Damage assessment of suspension footbridge using vibration measurement data combined with a hybrid bee-genetic algorithm. Scientific Reports, 12 (2022) 20143. doi:10.1038/s41598-022-24445-6.

[56]- A. Zara, I. Belaidi, S. Khatir, A. Oulad Brahim, D. Boutchicha, M. Abdel Wahab, Damage detection in GFRP composite structures by improved artificial neural network using new optimization techniques. Composite Structures, 305 (2023) 116475. doi:10.1016/j.compstruct.2022.116475.

[57]- N.P. Raut, A.B. Kolekar, S.L. Gombi, Optimization techniques for damage detection of composite structure: A review. Materials Today: Proceedings, 45 (2021) 4830-4834. doi:10.1016/j.matpr.2021.01.295.

[58]- D. Chen, Y. Li, A development on multimodal optimization technique and its application in structural damage detection. Applied Soft Computing, 91 (2020) 106264. doi:10.1016/j.asoc.2020.106264.

[59]- X. He, M. Kawatani, T. Hayashikawa, H. Furuta, T. Matsumoto, A Bridge Damage Detection Approach using Train-Bridge Interaction Analysis and GA Optimization. Procedia Engineering, 14 (2011) 769-776. doi:10.1016/j.proeng.2011.07.097.

[60]- Y. Lan, Y. Zhang, W. Lin, Diagnosis algorithms for indirect bridge health monitoring via an optimized AdaBoost-linear SVM. Engineering Structures, 275 (2023) 115239. doi:10.1016/j.engstruct.2022.115239.

[61]- N. Duong, V.L. Ho, T. Bui Tien, G. De Roeck, M. Abdel Wahab, Damage Evaluation of Free-Free Beam Based on Vibration Testing. Applied Mechanics, 1 (2020) 142-152. doi:10.3390/applmech1020010.

[62]- MATLAB, Natick, Massachusetts: The MathWorks Inc. (2020).

[63]- M. Mitchell, An Introduction to Genetic Algorithms. MIT Press, Cambridge. 1998.

[64]- J. Kennedy, B. Obayyanahatti, Particle swarm Optimization. Vol. 4. 1942-1948 vol.4, 1995.

[65]- B. Obayyanahatti, J. Kennedy, A New Optimizer Using Particle Swarm Theory. 39-43, 1995.

[66]- X.-S. Yang, S. Deb, Cuckoo Search via Levy Flights. (2010).